ANALYSIS OF A FLAT CAPILLARY EVAPORATOR WITH A BI-LAYERED POROUS WICK

***Paulo H. D. SANTOS*[1]*, Thiago A. ALVES*[*2]*, Amir A. M. OLIVEIRA*[3] *and Edson BAZZO*[3]

[1]Federal University of Technology – Paraná (UTFPR), Mechanical Engineering, Curitiba/PR, Brazil

[2]Federal University of Technology – Paraná (UTFPR), Mechanical Engineering, Ponta Grossa/PR, Brazil

[3]Federal University of Santa Catarina (UFSC), Mechanical Engineering, Florianóplois/SC, Brazil

*Corresponding author; E-mail: thiagoaalves@utfpr.edu.br

A numerical evaluation of the heat and mass transfer concerning a flat capillary evaporator provided by a bi-layered porous wick is presented. The wick has a shape of a flat disc and is assembled between the liquid feeding channel and the vapor chamber. An external heat input is applied into the upper surface of the bi-layered wick, where the working fluid evaporates. The mass and heat transfer are modeled using the mass and energy conservation equations. The model allows to verify the effect of design variables, such as working fluids, dimensions, permeability, average pore radius and thermal conductivity of the wick, in the performance of the capillary evaporator. It can be used as a predictive tool to design similar capillary pumping systems for thermal control of satellite or electronics systems in general.

Keywords: Flat Capillary Evaporator, CPL, Bi-layered Wick.

1 Introduction

The heat transfer analysis of the operation of the capillary evaporators have provided impotant phenomenological and design information. Demidov and Yatsenko [1] reported a theoretical investigation of the heat and mass transfer in the porous wick of capillary pumping systems. A numerical solution of the mathematical model was developed for studying the displacement of the evaporation front as the thermal load of the system increases. The same problem was also studied by Figus et al. [2]. They applied two models, a continuum volume-averaged formulation and a pore network model, for similar boundary conditions as those used by Demidov and Yatsenko [1] and assuming no pressure jump at the evaporation front.

Cao and Faghri [3] presented analytical solutions for the velocity and temperature fields for a similar problem, however subjected to different boundary conditions. They considered a completely liquid-saturated wick, with the evaporation front located in the outer surface, heated by an isothermal fin. Cao and Faghri [4] reported an extension of their previous work presenting a numerical analysis of a three-dimensional geometry.

Takahashi et al. [5] analyzed the heat and mass transfer with phase change in a cylindrical porous wick of a capillary evaporator. They assumed the same criterion developed in Figus et al. [2] which is based on the available area for evaporation. Contrary to Figus et al. [2], they included the capillary pressure jump at the liquid-vapor interface obtained from a static drainage curve and mercury porosimetry measured for a nickel sintered porous wick ($r_c = 1.6$ μm, $\varepsilon = 0.53$).

Kaya and Goldak [6] studied numerically the heat and mass transfer in the capillary porous structure and the boiling limit for a loop heat pipe (LHP). Depending on the heat flux supplied to the wick, the evaporation front was located at the outter surface of the porous structure or within it.

Although the works cited above provided the basis of the heat and mass transfer in capillary porous wicks, there is a lack of a comprehensive model that can predict the onset of drying at the fin/wick interface by capillary and boiling limits from consideration of the thermal and hydraulic properties of the working fluid and porous wick. Here, a fully liquid saturated wick bi-layered, in the shape of a flat disc, assembled between the liquid feeding channel and the vapor chamber, is considered.

2 PROBLEM FORMULATION

The geometry of interest here is shown in Fig. 1(a). This figure depicts a capillary evaporator with a bi-layered porous wick of a CPL. In this work, the wick is a flat circular disc and is assembled between the liquid feeding channel and the vapor chamber. The upper part of the wick is heated by an external heat flux. After start-up, the evaporation of the working fluid that takes place around the fin occurs in three regimes, depending on the magnitude of the applied heat flux: (1) evaporation in microfilm, (2) evaporation in the external surface of the wick and (3) evaporation within the wick. Here, the evaporation in the external surface of the wick is considered the normal operation mode of a CPL, as verified by Li and Ochterbeck [7] and assumed also by Cao and Faghri [3].

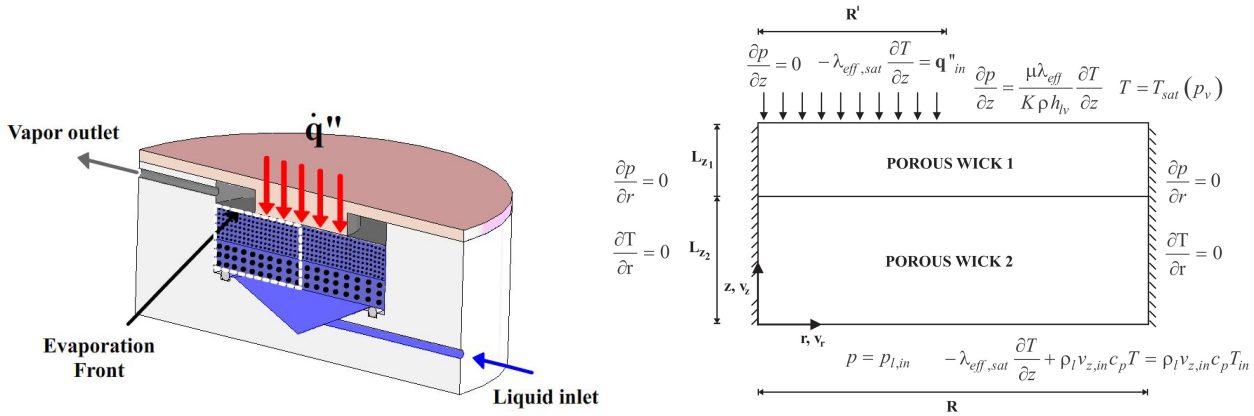

Figure 1 – (a) Cut of the flat capillary evaporator with bi-layered wick in the shape of a flat disc and (b) Schematic diagram of the calculation domain and the boundary conditions.

Here, the equations of conservation of energy and mass are cast in cylindrical coordinates and the physical domain of interest and the boundary conditions are represented schematically in Fig. 1(b). Due to the cylindrical symmetry, only the section represented by a dotted line in Fig. 1(a) is modeled.

The volume-averaged equation for the conservation of mass of liquid in cylindrical coordinates is

$$\frac{1}{r}\frac{\partial}{\partial r}\left(rv_r\right)+\frac{\partial v_z}{\partial z}=0. \tag{1}$$

Here, the volume averaged notation is omitted for simplicity. The formulation of the conservation of linear momentum depends on the flow velocity.Neglecting the influence of gravity, the r and z components of the equation for the conservation of linear momentum reduce to Darcy's Law, i.e.,

$$v_r = -\frac{K}{\mu}\frac{\partial p}{\partial r}, \quad v_z = -\frac{K}{\mu}\frac{\partial p}{\partial z}. \tag{2}$$

Substituting the conservation of momentum in the conservation of mass and assuming constant properties, we obtain a Laplace equation for the pressure, i.e.,

$$\frac{1}{r}\frac{\partial}{\partial r}\left(r\frac{\partial p}{\partial r}\right) + \frac{\partial}{\partial z}\left(\frac{\partial p}{\partial z}\right) = 0. \tag{3}$$

The equation for the conservation of the thermal energy is also written neglecting the convective terms. Following Cao and Faghri [3], the characteristic Peclet number (Pe$= \mathrm{Re}\,\mathrm{Pr} = v_{z,in}R^{'}/\alpha_e$) for the application of interest here is of the order of 10^{-2}. Then, the equation for the conservation of thermal energy, assuming isotropic media and constant properties, is written as

$$\frac{1}{r}\frac{\partial}{\partial r}\left(r\frac{\partial T}{\partial r}\right) + \frac{\partial}{\partial z}\left(\frac{\partial T}{\partial z}\right) = 0. \tag{4}$$

Following Fig. 1(b), the boundary conditions are:

At the surface at $r = 0$, cylindrical symmetry requires that

$$\frac{\partial p}{\partial r} = 0 \quad \text{and} \quad \frac{\partial T}{\partial r} = 0. \tag{5}$$

At the surface at $r = R$, the boundary is assumed impermeable to liquid flow and adiabatic. Then,

$$\frac{\partial p}{\partial r} = 0 \quad \text{and} \quad \frac{\partial T}{\partial r} = 0. \tag{6}$$

At the inlet surface at $z = 0$, the porous wick is fed with a liquid flow with far end temperature $T_{l,in}$, i.e.,

$$p = p_{l,in} \ \text{ and } \ -\lambda_e\frac{\partial T}{\partial z} + \rho_l v_{z,in} c_p T = \rho_l v_{z,in} c_p T_{l,in}. \tag{7}$$

In the volume-averaged sense and assuming local thermal equilibrium between the liquid and solid phases, λ_e is the effective thermal conductivity of the fully liquid saturated porous medium. Finally, at the outlet surface, two sections are observed. First, underneath the metallic fin ($z = L_z, 0 \le r \le R^{'}$)

$$\frac{\partial p}{\partial z} = 0 \quad \text{and} \quad -\lambda_e\frac{\partial T}{\partial z} = q_f. \tag{8}$$

Second, assuming that the pore size is not extremely small, i.e., the wick is not a hygroscopic porous medium, from Kelvin's Law, the surface temperature is approximately equal to the vapor saturation temperature in the bulk of the vapor channel. Also, the conduction heat transfer from the fin is responsible for the liquid evaporation. Therefore, the boundary condition at the evaporation surface can be written as,

$$\frac{\partial p}{\partial z} = \frac{\mu\lambda_e}{K\rho_l h_{lv}}\frac{\partial T}{\partial z} \quad \text{and} \quad T = T_{sat}\left(p_v\right). \tag{9}$$

This set of boundary conditions closes the formulation. The total working fluid mass flow rate is given by

$$\dot{m}_{lv} = \left[\int_0^R \left(-\frac{K}{\mu} \frac{\partial p}{\partial z} \rho_l \right) r dr \right]_{z=0} \tag{10}$$

The pressure difference $(p_v - p_{l,in})$ corresponds to the total pressure loss of the CPL components. In all stable operation points, this pressure difference balances exactly the capillary pressure difference across the medium. The total heat transfer rate at the fin is responsible for the liquid evaporation at the outlet surface and part of it flows to the liquid channel. A total energy balance in the wick provides

$$Q_f = q_f A_f = Q_l + Q_{lv}, \tag{11}$$

where Q_f is the applied heat transfer rate at the fin surface.

The heat transfer rate to the liquid channel Q_l, following Eq. 8, is given by,

$$Q_l = \int_0^R \left(-\lambda_e \frac{\partial T}{\partial z} \right) r dr, \;\; at \;\; z = 0. \tag{12}$$

This heat transfer is responsible for raising the incoming flow temperature of the subcooled liquid $T_{l,in}$ to the inlet porous wick surface value $T(z = 0)$. When Q_l is large, the liquid in the channel can reach the onset of nucleate boiling which is also called a boiling limit for the CPL operation. The boiling limit of interest here is the dryout that occurs underneath the fin, by excess temperature. Assuming cylindrical capillaries, the maximum capillary pressure (Young-Laplace's equation) that the wick can withstand is therefore,

$$\Delta p_{cap,max} = p_v - p_{l,\min} = \frac{2\sigma}{r_p} \tag{13}$$

This maximum capillary pressure is related to the threshold for percolation of the non-wetting phase and is commonly identified as the wick bubbling pressure.

3 Nondimensional equations

Following Udell [8] (see also Kaviany [9]), the characteristic scales for pore size, capillary pressure and liquid velocity can be defined as:

$$\begin{aligned} d_{ref} &= (k/\varepsilon)^{1/2}, \quad p_{ref} = \frac{\sigma}{d_{ref}} = \frac{\sigma}{(k/\varepsilon)^{1/2}}, \\ v_{ref} &= \frac{k}{\mu_l} \frac{p_{ref}}{L_z} = \frac{k}{\mu_l} \frac{1}{L_z} \frac{\sigma}{(k/\varepsilon)^{1/2}} = \frac{(k\varepsilon)^{1/2}}{\mu_l} \frac{\sigma}{L_z}. \end{aligned} \tag{14}$$

For the heat transfer, the heat flux applied to the fin is taken as the reference value, $q_{ref} = q_f$. Then, to develop a characteristic temperature diference, we can assume that the fin temperature at $z = L_z, r = 0, T_f$, is related to the fin heat flux by a conduction shape factor S such as

$$q_f = \lambda_e S \Delta T_{ref} = \lambda_e S \left(T_f - T_v \right). \tag{15}$$

Therefore, it is possible to define a reference temperature difference by

$$\Delta T_{ref} = T_f - T_v = \frac{q_f}{\lambda_e S} \tag{16}$$

where an order of magnitude for S can be obtained later.

The nondimensionalization is completed defining the aspect ratios $\eta_1 = R^{'}/L_z$ and $\eta_2 = R/L_z$.

3.1 Non-dimensional variables and parameters

Based on the characteristic scales, scaled length, radius, pressure, velocity, temperature and heat flux are:

$$z^* = \frac{z}{L_z}, \quad r^* = \frac{r}{R}, \quad p^* = \frac{p}{p_{ref}} = \frac{p\left(k/\varepsilon\right)^{1/2}}{\sigma}, \quad v^* = \frac{v}{v_{ref}} = \frac{v\mu_l L_z}{\sigma\left(k\varepsilon\right)^{1/2}}$$

$$T^* = \frac{T - T_v}{\Delta T_{ref}} = \frac{\left(T - T_v\right)\lambda_e S}{q_f}, \quad q^* = \frac{q}{q_{ref}} = \frac{q}{q_f} \tag{17}$$

The boundary condition for the pressure of the liquid-phase, at $z = L_z, R^{'} \leq r \leq R$, produces the driving force for the capillary pumping. With the non-dimensionalization proposed it becomes

$$\frac{\partial T^*}{\partial z^*} = \mathrm{Ev}\frac{\partial p_l^*}{\partial z^*}, \tag{18}$$

where the evaporation-cooling number Ev is defined as

$$\mathrm{Ev} = \frac{\rho_l h_{lv}\sigma\left(k\varepsilon\right)^{1/2} S}{q_f \mu_l} \equiv \frac{\rho_l h_{lv}\sigma\left(k\varepsilon\right)^{1/2}}{\lambda_e\left(T_f - T_v\right)\mu_l}. \tag{19}$$

The evaporation-cooling number is the ratio between the absorbed as latent heat, by the evaporation of the capillary-pumped liquid flow and the conduction heat transfer rate across the porous wick from the fin to the evaporation surface. From the inlet boundary condition for the energy equation, $z = 0$, a characteristic Peclet number appears as

$$\mathrm{Pe} = \frac{\rho_l c_{p,l}\sigma\left(k\varepsilon\right)^{1/2}}{\lambda_e \mu_l} \tag{20}$$

From the non-dimensional variables defined above, the following non-dimensional equations are obtained:

Equation of conservation of thermal energy,

$$\frac{\partial^2 T^*}{\partial z^{*2}} + \frac{1}{\eta_2^2}\frac{\partial}{r^*\partial r^*}\left(r^*\frac{\partial T^*}{\partial r^*}\right) = 0, \tag{21}$$

Boundary conditions,

$$
\begin{aligned}
&z^* = 0, && -\frac{\partial T^*}{\partial z^*} + \mathrm{Pe} v_l^* T^* = \mathrm{Pe} v_l^* T_l^*, \\
&z^* = 1, && 0 \le r^* \le r'^*, \qquad \frac{\partial T^*}{\partial z^*} = SL_z; \\
& && r'^* \le r^* \le 1, \qquad T^* = 0 \\
&r^* = 0, && \frac{\partial T^*}{\partial r^*} = 0, \\
&r^* = 1, && \frac{\partial T^*}{\partial r^*} = 0
\end{aligned}
\tag{22}
$$

The nondimensional z and r heat fluxes are

$$
\begin{aligned}
q_z^* &= -\frac{1}{SL_z}\frac{\partial T^*}{\partial z^*} \\
q_r^* &= -\frac{1}{\eta_2 SL_z}\frac{\partial T^*}{\partial r^*}
\end{aligned}
\tag{23}
$$

Equation of conservation of linear momentum,

$$
\frac{\partial^2 p_l^*}{\partial z^{*2}} + \frac{1}{\eta_2^2}\frac{\partial}{r^* \partial r^*}\left(r^* \frac{\partial p_l^*}{\partial r^*}\right) = 0,
\tag{24}
$$

Boundary conditions,

$$
\begin{aligned}
&z^* = 0, && p_l^* = p_o^* \\
&z^* = 1, && 0 \le r^* \le r'^*, \qquad \frac{\partial p_l^*}{\partial z^*} = 0; \\
& && r'^* \le r^* \le 1, \qquad \frac{\partial p_l^*}{\partial z^*} = \frac{1}{\mathrm{Ev}}\frac{\partial T^*}{\partial z^*} \\
&r^* = 0, && \frac{\partial p_l^*}{\partial r^*} = 0 \\
&r^* = 1, && \frac{\partial p_l^*}{\partial r^*} = 0
\end{aligned}
\tag{25}
$$

The nondimensional z and r liquid velocities are

$$
\begin{aligned}
v_{l,z}^* &= -\frac{\partial p_l^*}{\partial z^*} \\
v_{l,r}^* &= -\frac{1}{\eta_2}\frac{\partial p_l^*}{\partial r^*}
\end{aligned}
\tag{26}
$$

The conservation equations were solved numerically by the finite volume method [10, 11]. The tri-diagonal matrix algorithm (TDMA) was employed to solve the discretized equations in a segregated form. The numerical algorithm can be summarized as:

1. An inlet velocity is estimated to solve the Laplace equation for the temperature. From the solution for T, the outlet velocity is calculated using the boundary condition given by Eq. (9).

2. The pressure equation is solved using the outlet velocity calculated in step (1). Then, the velocities are calculated and the values are compared to the ones used in step (1);

3. Return to step (1) until a converged solution is obtained.

The code verification was developed according to the method reported by Eça and Hoekstra [12], and it was found that a grid of (150 x 150) is sufficient to obtain accurate solutions. Convergence was examined by checking the overall mass and energy balances. The coupled equations are assumed to converge when overall energy and mass balances are satisfied within $\pm\ 1\%$.

4 Results and Discussion

The results are presented as follows. Three analyses are developed: analysis of the effect of the magnitude of the external heat transfer rate in the mass flow rate, analysis of the onset of drying (one-layer) and analysis of the effect of a bi-layered structure on the mass flow rate and onset of drying. For the results presented here, water was used as working fluid. A wick, initialy with one layer and next with two layers with different thermal properties, was used as porous wick. The thermodynamic properties of the wick and the working fluid and the nondimensional parameters are presented in Table 1.

Table 1 – Dimensions, properties of wick, fluid thermophysical properties and calculated reference and non-dimensional variables.

Dimensions and properties			Calculated variables		
Wick dimensions			Reference values		
R	mm	15	d_{ref}	m	26.46×10^{-6}
$R^{'}$	mm	7.5	p_{ref}	Pa	269111
L_z	mm	10	v_{ref}	m/s	1.18×10^{-3}
Fluid properties			ΔT_{ref}	K	10
ρ_l	kg/m^3	995.6	q_{ref}	W/m^2	4000
$c_{p,l}$	J/kg-K	4180	Non-dimensional variables		
μ_l	Pa.s	7.98×10^{-4}	η_1		0.75
σ	N/m	7.12×10^{-2}	η_2		1.5
h_{lv}	J/kg	2.382×10^6	p_s^*		0.027
$p_s(T_v)$	Pa	7299.45	Pe		12.28
Wick properties					
ε	nondim.	0.5			
r_p	μm	$3 - 15$			
K	m^2	35×10^{-15}			
$\lambda_{e,1}$	W/m-K	$4 - 8$			
$\lambda_{e,2}$	W/m-K	4			
T_v	^{o}C	40			
T_l	^{o}C	30			

4.1 Analysis of the Onset of Drying

The heat transfer rate imposed in the fin is transferred to the outlet surface, causing evaporation, and also to the inlet surface, resulting in heating of the liquid channel. Both these heat transfer paths have their characteristic thermal resistances. As a result of these thermal resistances, the fin surface reaches a temperature which can be reasonably large in certain conditions. The maximum capillary pressure that a pore with radius r_p can sustain is,$2\sigma/r_p$. The non-dimensional maximum capillary pressure is

$$\Delta p^*_{cap,max} = \frac{2\sigma\left(K/\varepsilon\right)^{1/2}}{\sigma r_p} = \frac{2\left(K/\varepsilon\right)^{1/2}}{r_p}. \tag{27}$$

Note that this maximum nondimensional capillary pressure is a purely geometrical parameter. When applied to a porous wick, this means that the maximum capillary pressure is the one that occurs when the average radius of the curvature of all menisci exposed to the vapor phase is equal to r_p.

The local nondimensional capillary pressure at the outlet surface is given by,

$$\Delta p^*_{cap} = \frac{\left(p_v - p_l\right)\left(K/\varepsilon\right)^{1/2}}{\sigma} \tag{28}$$

where $p_v = p_{sat}(T_v)$ and p_l is obtained from the solution of the model, $p_l = p_l(r)$ at $z = L_z$.

Fig. 2(a) presents the nondimensional capillary pressure at the top surface as a function of properties for two heat fluxes, $q^*_f = 10.5$ and $q^*_f = 5.0$. All properties were kept constant and correspond to the properties of the porous wick with nondimensional average pore radius of 11.34. The horizontal lines represent the maximum nondimensional capillary pressure for each characteristic nondimensional pore size. Nondimensional pore size from 11.34 to 56.69 as shown. We note that for the nondimensional inlet heat flux of 5.0 all media would remain saturated by liquid except those with the larger nondimensional pores of 37.80 and 56.69.

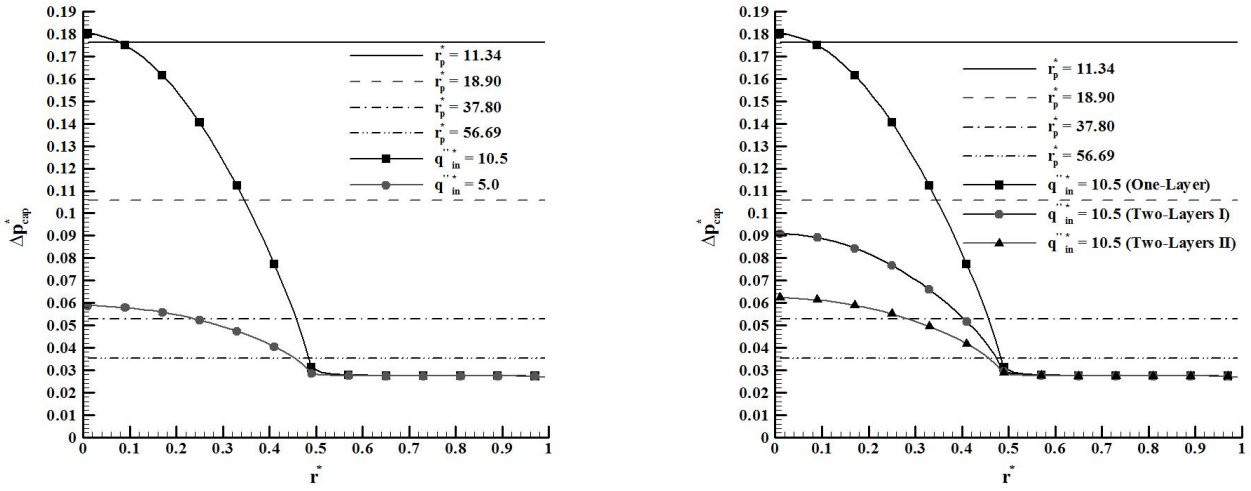

(a) (b)

Figure 2 – (a) Nondimensional capillary pressure profiles at $z^* = 1.0$ for nondimensional inlet heat fluxes for one layer and (b) bi-layered wick.

For higher heat flux, all media with pore sizes above 11.34 would suffer dry out underneath the fin. Therefore, there is a relation between the pore size (and all medium properties) and the heat flux at the onset of drying. Note that this drying underneath the fin may not cause the failure by the capillary limit, since there may be a stable condition for operation with the embedded evaporation front according to Demidov and Yatsenko [1], Figus et al. [2], Takahashi et al. [5], Kaya and Goldak [6]. This, however, is not analyzed here. Nevertheless, this test allows the definition of safe operation limits.

4.2 Analysis of the Onset of Drying in the Bi-layered Structure

Here, the analysis of the porous wick with two layers is presented. It is expected that this kind of porous structure improves the capillary pumping capacity, avoiding reaching the capillary limit. It is also expected that the heat transfer to the feeding liquid channel is decreased. For the bi-layered porous wick, porous wick 1 and 2 have nondimensional lengths of $L^*_{z,1} = 0.4$ and $L^*_{z,2} = 0.6$, respectively. The porous wick 2 has the effective thermal conductivity constant ($\lambda_{e,2} = 4.0$ W/mK). The effective thermal conductivity of the porous wick 1 was varied ($\lambda_{e,1}$) from 4.0 to 8.0 W/mK in order to evaluate its effect on the onset of drying.

Figure 2(b) presents the nondimensional capillary pressure at the top surface as a function of properties of the wicks with one and two layers for a nondimensional inlet heat flux of 10.5 and four characteristic nondimensional pore average radius (from 11.34 to 56.69). All properties were also kept constant and correspond to the nondimensional average porous radius of 11.34. Note that for the nondimensional inlet heat flux of 10.5 in the wick with two layers, as the thermal conductivity increase the local capillary pressure decreases and may not exceed the maximum allowed capillary pressure.

For a given nondimensional heat flux there will be a minimum nondimensional average radius needed to avoid the drying of the wick in the region underneath the fin, which will be called critical nondimensional average radius ($r^*_{p,crit}$). This is given by,

$$r^*_{p,crit} = \frac{2\sigma}{(p_v - p_l)\,(K/\varepsilon)^{1/2}} \tag{29}$$

where $p_v = p_{sat}(T_v)$ and p_l is the local value of liquid pressure calculated from the model, $p_l = p_l(r)$ at $z = L_z$. Here, $\sigma = \sigma(T)$ where T is the porous wick temperature.

Figure 3 presents curves of critical nondimensional average radius as a function of the nondimensional heat flux in the upper part of the wick ($z^* = 1$) for a wick with one- and two-layers. Figure 3(a) presents the nondimensional critical average radius for two nondimensional heat fluxes (5.0 and 10.5). This is the same condition presented in Fig. 2(a) and (b). Note that, in the region underneath of the fin, the smaller the nondimensional heat flux the higher the critical nondimensional average radius. That is, the temperatures underneath the fin and the mass flow rate decrease with the decreasing of heat flux. As a consequence the capillary pressure also decreases. Since the critical average radius is inversely proportional to the maximum capillary pressure according Eq. (29), when the nondimensional heat flux is decreased the critical nondimensional average radius increases. For the nondimensional heat flux of 10.5 the porous wick should be manufactured with minimum critical nondimensional average radius of 10.86 ($r_p = 2.87$ μm, calculated for the properties from Table 1), while for nondimensional heat flux of 5.0 it is sufficient a minimum critical nondimensional average radius of 32.18 ($r_p = 8.51$ μm, calculated for the properties from Table 1).

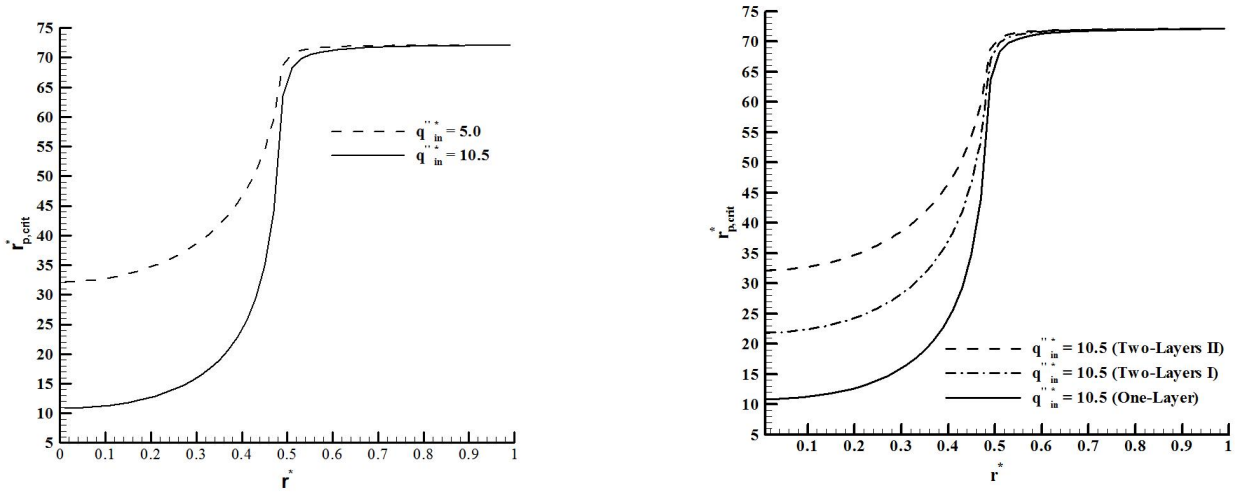

(a) (b)

Figure 3 – (a) Critical nondimensional average radius profiles at $z^* = 1.0$ for nondimensional inlet heat fluxes for one layer and (b) bi-layered wick.

It is noted in Fig. 3(b) that for the same nondimensional heat flux of 10.2, as the thermal conductivity of the wick 1 increases, the minimum critical nondimensional average radius also increases in the region underneath of the fin. The minimum critical nondimensional average radius is 32.18 (two-layers II - $\lambda_{e,1} = 8.0$ W/mK), 21.86 (two-layers I - $\lambda_{e,1} = 6.0$ W/mK) and 10.86 (one-layer). Therefore, these results provide guidelines for the design and manufacture of the porous wicks in order to avoid the drying of the region underneath the fin.

It is noticed in Fig. 3 that the minimum critical nondimensional average radius is located in the region underneath of the fin at $z^* = 1.0$ and $r^* = 0.0$. Thus, the Fig. 4 presents the critical nondimensional average radius as a function of the nondimensional heat flux at this location ($z^* = 1.0$ and $r^* = 0.0$).

Figure 4 presents the minimum critical nondimensional average radius ($r^*_{p,crit}$) as a function of the nondimensional heat flux for a wick with one (Fig. 4(a)) and two layers (Fig. 4(b)). The curves shown in these figures represent the capillary limit, *i.e.*, bellow the curves the capillary limit is not reached and there is no vapor breakthrough and above the curves occurs the vapor invasion of the porous wick. Note in (Fig. 4(b) that, as the thermal conductivity of the wick 1 increases, the capillary limit is displaced and the minimum critical nondimensional average radius also increases. For a minimum critical nondimensional average radius of 20, for instance, the nondimensional heat flux increases from 7.5 (one layer) to 15 (two layers) which refer to a heat flux of 3×10^4 W/m^2 and 6×10^4 W/m^2, respectively.

5 Conclusions

The model developed here allowed to verify the effect of design variables in the steady-state performance of a flat capillary evaporator. The analysis of the wick with one and two layers showed that the wick with two layers is better than with one layer regarding the onset of drying underneath the fin. Thus the capillary limit, or onset drying, has a relation between the pore size (and all medium properties) and the heat flux. If this

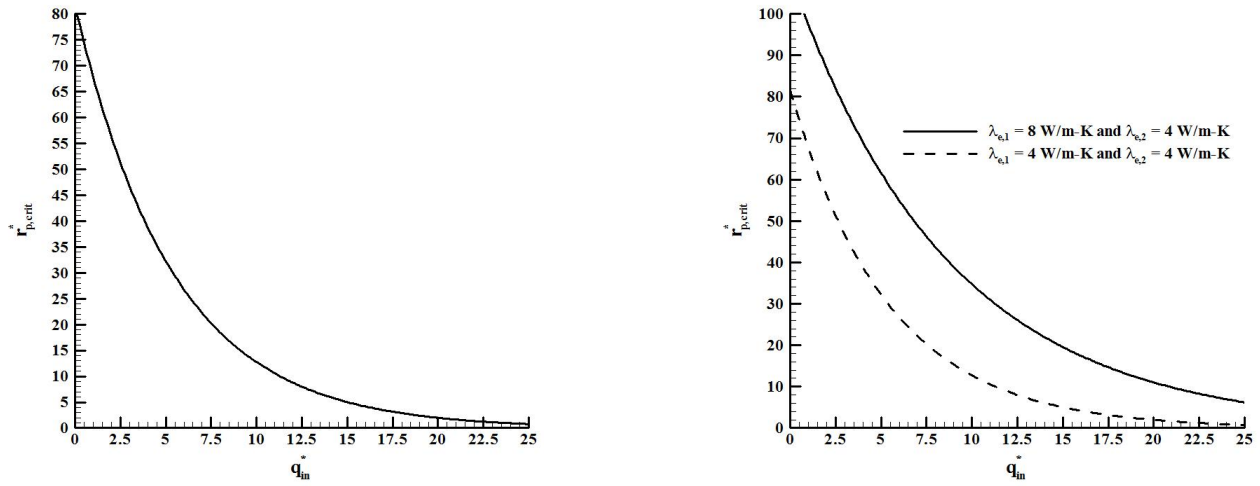

(a) (b)

Figure 4 – (a) Minimum critical nondimensional average radius at $z^* = 1.0$ and $r^* = 0.0$ as a function of the nondimensional inlet heat flux for one layer and (b) bi-layered wick.

limit is reached, the evaporation front may penetrate within the wick. This can be used as a criterium for the specification of the maximum heat flux allowed during operation in steady-state.

The larger the thermal conductivity of the porous wick 1 (underneath the fin), the smaller is the heat transfer to the feeding channel, causing a smaller increase of the inlet temperature. The increase of the thermal conductivity of the porous wick 1 causes the increase of the capillary limit, avoiding the onset drying of the region underneath the fin. The increase of the thermal conductivity also decreases the mass flow rate, causing the decrease of the pressure losses through the porous wick.

Finally, the dimensions of the bi-layered wick ($R = 15$ mm, $R^{'} = 7.5$ mm, $L_{z,1} = 4$ mm, $L_{z,2} = 6$ mm) and its thermophysical properties can be used for a design of a flat capillary evaporator.

References

[1] A. S. Demidov and E. S. Yatsenko. Investigation of heat and mass transfer in the evaporation zone of a heat pipe operating by the inverted meniscus principle. *International Journal of Heat and Mass Transfer*, 37:2155–2163, 1994.

[2] C. Figus, Y. L. Bray, S. Bories, and M. Prat. Heat and mass transfer with phase change in a porous structure partially heated: continuum model and pore network simulation. *International Journal of Heat and Mass Transfer*, 42:2557 –2569, 1999.

[3] Y. Cao and A. Faghri. Analytical solution of flow and heat transfer in a porous structure with partial heating and evaporation on the upper surface. *International Journal of Heat and Mass Transfer*, 37: 1525 – 1533, 1994.

[4] Y. Cao and A. Faghri. Conjugate analysis of a flat-plate type evaporator for capillary pumped loops with three-dimensional vapor flow in the groove. *International Journal of Heat and Mass Transfer*, 37: 401–409, 1994.

[5] A.R. Takahashi, A. A. M. Oliveira, and E. Bazzo. Analysis of heat and mass transfer with pphase change in the porous wick of a capillary pump. In *7th International Heat Pipe Symposium, Jeju Korea*, 2003.

[6] T. Kaya and J. Goldak. Numerical analysis of heat and mass transfer in the capillary structure of a loop heat pipe. *International Journal of Heat and Mass Transfer*, 49:3211–3220, 2006.

[7] T. Li and J. M. Ochterbeck. Effect of wick thermal conductivity on startup of a capillary pumped loop evaporator. *AIAA*, 993446:10–20, 1999.

[8] K. S. Udell. Heat transfer in porous media heated from above with evaporation, condensation and capillary effects. *ASME*, 105:485–492, 1983.

[9] M. Kaviany. *Principles of Heat Transfer in Porous Media*. Springer-Verlag, 1995.

[10] S. V. Patankar. *Numerical Heat Transfer and Fluid Flow*. Hemisphere Publishing Corporation, 1980.

[11] C. R. Maliska. *Heat Transfer and Computational Fluid Mechanics (In portuguese)*. Scientific and Technical Books, 2004.

[12] L. Eça and M. Hoekstra. Code verification of unsteady flow solvers with method of manufactured solutions. *International Journal of Offshore and Polar Engineering*, 18:120–126, 2008.

6 Nomenclature

c_p	specific heat	[J/kg-K]	**Greek Symbols**		
Ev	evaporation-cooling number	[-]	α	thermal diffusivity	$[\mathrm{m}^2/\mathrm{s}]$
h_{lv}	latent heat of evaporation	[J/kg]	ϵ	porosity	
K	permeability	$[\mathrm{m}^2]$	λ	thermal conductivity	[W/m-K]
L	wick thickness	[m]	μ	dynamic viscosity	[Pa-s]
$\dot{m}$	mass flow rate	[kg/s]	ρ	mass density	$[\mathrm{kg}/\mathrm{m}^3]$
p	pressure	[Pa]	σ	surface tension	[N/m]
Pe	Peclet number	[-]	θ	contact angle	[rad]
q	heat flux	$[\mathrm{W}/\mathrm{m}^2]$	**Subscripts**		
$\dot{Q}$	heat transfer rate	[W]	cap	capillary	
$R^{'}$	fin radius	[m]	e	effective	
R	wick external radius	[m]	f	fin, fin/wick interface	
Re	pore Reynolds number	[-]	in	inlet	
r_p	pore radius	[m]	l	liquid, liquid side	
T	temperature	[K]	sat	saturation	
v	liquid velocity	[m/s]	v	vapor	